ELSEVIER

Journal of Chromatography B, 741 (2000) 243–255

JOURNAL OF CHROMATOGRAPHY B

www.elsevier.com/locate/chromb

Analysis of gamma radiation-induced damage to plasmid DNA using dynamic size-sieving capillary electrophoresis

Stacey A. Nevins[a,1], Barbara A. Siles[a,*], Zeena E. Nackerdien[b,2]

[a]*Department of Chemistry, The College of William and Mary, P.O. Box 8795, Williamsburg, VA 23187-8795, USA*
[b]*Biotechnology Division, National Institute of Standards and Technology, Gaithersburg, MD 20899, USA*

Received 24 September 1999; received in revised form 25 January 2000; accepted 31 January 2000

Abstract

Bacterial plasmids and the chromosomal DNA of many organisms adopt naturally the negatively supercoiled conformation. Therefore, the irradiation of such plasmids could be used to model conformational changes of chromosomal DNA associated with externally-induced damage. We have applied dynamic size-sieving capillary electrophoresis (CE) to monitor the damage of three DNA plasmids, over an unprecedented base pair (bp) size range (2870–27 500 bp), upon exposure to γ-radiation (20–400 Gy). Predominantly, CE with UV absorbance detection in the absence of DNA intercalating dyes was employed to preclude undesirable, induced plasmid conformational changes. Plasmid samples and their enzymatic digestion products were analyzed using both CE and slab gel electrophoresis (SGE) in order to verify the conformation of sample components. Relative to SGE, CE analyses revealed more fine structural features of plasmid degradation.

Keywords: Plasmids; Gamma-radiation; DNA

1. Introduction

Plasmids are naturally occurring, circular double-stranded DNA (dsDNA) molecules that replicate independently of the genome. Many plasmids encode unique metabolic functions such as resistance to antibiotics, heavy metals or UV radiation. In the cell, bacterial plasmids adopt a negatively supercoiled conformation. Large plasmids and chromosomal DNA are organized into discrete topological domains with defined numbers of supercoils and helical turns. These supercoils are critical to the regulation of several biological processes, including DNA replication and gene expression [1]. Other possible plasmid conformations include the open circular conformer (either the relaxed form or the nicked form) and the linear conformer. The nicked open circular form is generated by a single-stranded break (a nick), which allows supercoiled DNA to unwind [1,2]. Breaks may be induced by (i) brief treatment with restriction endonucleases, (ii) radical processes mediated by reactive oxygen species, (iii) ionizing radiation, or

*Corresponding author. The University of Denver Research Institute, 2050 E. Iliff Ave., Denver, CO 80208, USA. Tel.: +1-303-8717-464, fax: +1-303-8714-119.

E-mail address: bsiles@du.edu (B.A. Siles)

[1]Present address: Department of Chemistry, The University of Michigan, 930 N. University, Ann Arbor, MI 48109-1055, USA.

[2]Present address: Qualus, 420 East 51 Street, Suite A, New York, NY 10022, USA. Tel.: +1-212-2230-813; fax: +1-212-2230-893.

0378-4347/00/$ – see front matter
PII: S0378-4347(00)00106-7

(iv) laser photolysis [3–6]. The linear conformer can be generated by a double-stranded break via digestion with a restriction endonuclease, or by two closely opposed single-strand breaks [1,2,4].

The analysis of DNA fragmentation due to ionizing radiation is critical to the development of more effective radiation therapies. Two established techniques for DNA fragmentation analysis are the comet assay (single cell gel assay) and slab gel electrophoresis (SGE). The comet assay is used to monitor DNA damage in individual nuclei; the name is derived from the characteristic band ''tailing'' during electrophoresis of small DNA fragments from the nucleus [7,8]. SGE allows for the comparison of several DNA samples simultaneously, but quantitation of the conversion of plasmid conformers is complicated by the differential binding of intercalating dyes to DNA molecules. These dyes also induce conformational changes in circular DNA, as demonstrated by Johnson and Grossman [3]. Sutherland et al. have developed a normalization technique to compensate for these differences, which was used for the quantitation of plasmid conformational changes upon irradiation [4].

The high separation efficiency of capillary electrophoresis (CE) makes it a viable alternative to SGE for the analysis of radiation damage to DNA. Previous studies by Siles et al. have demonstrated the detection of γ-irradiated linear dsDNA fragments and genomic DNA using dynamic size-sieving CE [5]. Nackerdien et al. investigated the laser-induced photolysis of DNA plasmids in either the presence or absence of ethidium bromide using CE [6]. In the latter investigation, the irradiation of the DNA plasmid molecules in the presence of the intercalating dye, ethidium bromide, was more effective in the conversion of the supercoiled confomer into nicked conformers. In general, the incorporation of DNA intercalating dyes into the CE dynamic size-sieving buffer can enhance the separation and detection of DNA molecules. However, the presence of such intercalating dyes within the separation matrix may induce, simultaneously, undesirable conformational changes in DNA plasmid molecules. Recently, Mao et al. have demonstrated the analysis of the linear, supercoiled and nicked conformers of the pBR322 plasmid using CE with native UV absorbance detection at 260 nm in the absence of intercalating dyes [9]. Using this mode of detection, analyses were highly representative of the injected samples.

In the present study, we have investigated the use of CE to monitor the nicking and fragmentation of bacterial plasmids exposed to γ radiation in the absence of intercalating dyes. Three plasmids, ranging in size from 2870 base pairs (bp) to 27 500 bp, were analyzed using dynamic size-sieving CE; individual peaks were sized relative to linear and supercoiled plasmid DNA standards. Samples were analyzed concurrently using SGE to aid in conformer identification. Previous CE investigators have not examined irradiated plasmid molecules larger than 4 kbp. We have separated fragmentation products using CE in dilute size-sieving polymer solutions not containing intercalating dyes. Previous CE analyses of irradiated plasmids have incorporated DNA intercalating dyes into the separation medium in the analysis of linear, supercoiled and nicked plasmid conformers [6]. The latter may cause the aforementioned, undesirable plasmid conformational changes. As the negatively supercoiled form is the natural state of bacterial plasmids and the chromosomal DNA of many organisms, the adaptation of the present investigation to the single-cell analysis CE format could potentially model the conformational changes of cellular chromosomal DNA upon externally-induced damage.

2. Experimental

2.1. CE methodology

2.1.1. Instrumentation

A CE system with UV absorbance detection (the CE–UV system) was assembled in the laboratory. This system consisted of a Spellman CZE1000R power supply (High Voltage Electronics, Hauppauge, NY, USA) with platinum–iridium electrodes, and a Unicam 4225 UV–Vis detector (Philips Scientific, Cambridge, UK). The inlet buffer reservoir was connected to a pressure block fitted with a nitrogen line. The capillary was cooled using forced air convection via two 22 W fans. Room temperature of the laboratory was typically 21°C. A second CE system with laser-induced fluorescence detection (the CE–LIF system) was also assembled in the labora-

tory. This system consisted of an Advanced Technologies (ATI, Boston, MA, USA) Unicam Crystal 300 CE unit and a Spectrovision FD-300 Dual Monochromator fluorescence detector (Groton Technologies, Concord, MA, USA). The temperature of the ATI CE system was maintained at 30.0±0.1°C using a Peltier heating–cooling system. The fluorescence detector was mounted on an optical bench and retrofitted with a single line (488 nm), air-cooled argon ion laser (Uniphase, San Jose, CA, USA) as the light source. A mirror mounted on the optical bench was used to direct the laser light through a lens (Melles Griot, Irvine, CA, USA), which focused the light on the capillary detection window. Emitted light passed through a 520 nm cut-off filter. Data points from both CE systems were taken every 100 ms and recorded using Axxiom Chromatography Model 737 data acquisition software (Moorpark, CA, USA).

2.1.2. Capillaries and capillary treatment

Bare fused-silica capillaries of 50 μm I.D.×361 μm O.D. were employed (Polymicro Technologies, Tucson, AZ, USA). Initial capillary pretreatment entailed a 4-h rinse with 0.1 *M* HCl, followed by a 30-min rinse with HPLC-grade water at 2760 mbar. Capillary conditioning between analyses was alternated between a 10 min and 20 min rinse with 1.0 *M* HCl at 6900 mbar, followed by a 5 min rinse with HPLC-grade water at 6900 mbar. For the ATI LIF system, solutions were transported through the capillary at the maximum suggested pressure of the ATI unit, 2000 mbar. These rinsing procedures were adapted from Fung and Yeung, and nearly eliminate electroosmotic flow in the capillary [10]. The in-laboratory analysis of the neutral marker mesityl oxide yielded an electrophoretic mobility of $9.50 \cdot 10^{-6}$ cm^2 V^{-1} s^{-1} [11]. A 40 cm capillary (23 cm effective length) was used in the CE–UV system; a 60 cm capillary (41 cm effective length) was used in the CE–LIF system.

2.1.3. Preparation of polymer solutions

Hydroxyethylcellulose (HEC) with a molecular mass distribution of 90 000–105 000 g/mol (Polysciences, Warrington, PA, USA) was used as received, and is referred to hereafter as HEC-90K. Polymer solutions were prepared by adding the dry polymer to Tris–HCl–EDTA (THE) buffer at a concentration of 0.30% (w/w). THE buffer solution was composed of 89 m*M* Trizma base (Sigma, St. Louis, MO, USA), 89 m*M* HCl (Fisher Scientific, Fair Lawn, NJ, USA) and 2 m*M* Na_2EDTA (Sigma), and was adjusted to pH 7.3 using a saturated KOH solution. Buffer solutions were vacuum filtered through a 0.5-μm cellulosic filter (MSI, Westborough, MA, USA) via water aspiration prior to adding the polymer. Polymer solutions were heated in a microwave oven and shaken mechanically; HPLC-grade water was added gravimetrically to replace water lost during heating. Each polymer solution was vacuum filtered through a 5-μm cellulosic filter (MSI). In CE–LIF analyses, YO-PRO-1 intercalating dye (Molecular Probes, Eugene, OR, USA) was added to polymer solutions at a concentration of 100 ng/ml.

2.1.4. Electrophoretic analyses

For the CE–UV system, polymer solutions were loaded into the capillary for 4–6 min at 2760 mbar and pre-electrophoresed at −550 V/cm until a current of −102 μA was reached. This initial electrophoresis step was used to remove ionic impurities [10] and enhance the reproducibility of analyses [12]. Samples were injected at −1 kV to −5 kV for 3 to 10 s, and the applied run voltage was −15 kV for a resulting field strength of −375 V/cm. For the CE–LIF system, polymer solutions were loaded into the capillary for 6 min at 2000 mbar and pre-electrophoresed at −367 V/cm for 1 min. Samples were injected at −2 kV for 0.17 to 0.34 min. The applied run voltage was −15 kV, for a resulting field strength of −250 V/cm.

2.2. Slab gel electrophoresis

Slab gel electrophoretic separations were performed using a submarine apparatus (E-C Apparatus, Holbrook, NY, USA). Gels of Trevigel 500 (Trevigen, Gaithersburg, MD, USA) were prepared at a concentration of 0.50% (w/w) using either TAE buffer (40 m*M* Tris–acetate–2 m*M* Na_2EDTA, pH 8.5) or THE buffer (89 m*M* Tris–HCl–2 m*M* Na_2EDTA, pH 8.5), as indicated. The polymer solutions were heated in a microwave oven and shaken mechanically; HPLC-grade water was added

gravimetrically in order to replace water lost during heating. The applied run voltage was 103 V (12.1 V/cm); 0.1–1.0 μg of each sample was loaded. Bands were stained after separation in a buffer solution containing 0.5 μg/ml ethidium bromide. Gels were destained for 30 min using HPLC-grade water, and bands were visualized using an UV-transilluminator (Fisher Scientific).

2.3. Sample preparation

2.3.1. DNA samples

The pTZ19R plasmid (2870 bp) and the 2′-deoxyguanosine-5′-triphosphate (dGTP) internal standard were donated by Trevigen. The ΦX174 plasmid (5386 bp), 1 kilobase pair (1 kbp) ladder standard (75 bp–12 kbp), and supercoiled ladder standard (2–16 kbp) were purchased from Life Technologies (Gaithersburg, MD, USA). The 1500 bp linear dsDNA internal standard was purchased from Gensura Labs. (Del Mar, CA, USA). The pMD68 plasmid (27.5 kbp) was prepared by Dr. M. Daley of the Uniformed Services University of the Health Sciences (Bethesda, MD, USA). Samples were diluted to 10–50 ng/μl with HPLC-grade water, and the internal standards were added at ratios of 1:10 (dGTP:DNA) and 1:10 (1500 bp:DNA) as indicated.

2.3.2. Enzymatic digestions

The linear conformer of the ΦX174 plasmid was generated by digestion with *Xho*I restriction endonuclease (Promega, Madison, WI, USA) at 37°C for 10 min according to the directions of the supplier. The linear conformer of the pTZ19R plasmid was produced by digestion with *Eco*RI restriction endonuclease (Pharmacia, Piscataway, NJ, USA) at 37°C for 10 min according to the directions of the supplier. Linearized samples were purified using the Trevigen Apoptotic Laddering Kit (Trevigen) according to the directions of the manufacturer. *Eco*RI digestions of the pTZ19R plasmid were also performed at 0°C for up to 15 min to generate multiple conformers; reactions were halted by the addition of Na_2EDTA to a final concentration of 0.02 m*M*.

2.3.3. Irradiation

Irradiated samples were exposed to a γ-^{60}Co source at a rate of 58.2 Gray (Gy)/min (1 Gy=100 rads of radiation). The pTZ19R and ΦX174 samples were irradiated at doses of 50, 100 and 200 Gy; the internal standard, dGTP, was added after irradiation. All irradiations were performed in the presence of air. The pMD68 sample was irradiated at 20, 200 and 400 Gy. Irradiated samples were stored in a −80°C freezer. Between electrophoretic analyses, samples were placed in a benchtop Nalgene cooler (stored prior to use at −80°C), with a bench top temperature of less than −20°C (Nalge, Rochester, NY, USA).

3. Results and discussion

3.1. Analysis of the ΦX174 plasmid sample

Initially, the ΦX174 plasmid sample was analyzed as received using SGE to identify the conformers present; two bands were observed (Fig. 1, lane 2). Electrophoretic bands within each lane will be referred to hereafter in order of decreasing electrophoretic mobility, with band 1 having the greatest mobility. Calibration plots of migration distance versus DNA size in bp were constructed using the 1 kbp and supercoiled ladder standards (data not shown). Sizing based on the calibration plot constructed from the supercoiled ladder standard suggested that band 1 of the original ΦX174 plasmid sample (lane 2) was the supercoiled monomer (calculated size: 5363 bp, actual size: 5386 bp). Band 2 did not correspond to a multiple of the monomer size, reducing the likelihood of supercoiled multimers as possible structures. We suggest that band 2 of the original ΦX174 sample represents the nicked/open circular form. The migration order of the supercoiled and nicked/open circular conformers agrees with that cited previously using SGE for the ΦX174 plasmid [3]. This nicked/open circular form may have been produced by single-stranded breaks during freeze–thaw cycles between cold storage and use, as well as radical processes mediated by reactive oxygen species. To minimize further nicking, the ΦX174 plasmid sample was aliquotted into several tubes, so that each stock solution was subjected to fewer freeze–thaw cycles and reduced exposure to oxygen in the atmosphere. Relative band intensities in lane 2 suggest that the original ΦX174 plasmid sample exists predominantly in the supercoiled con-

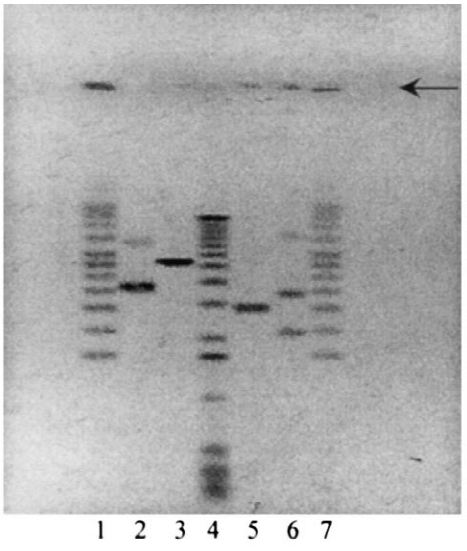

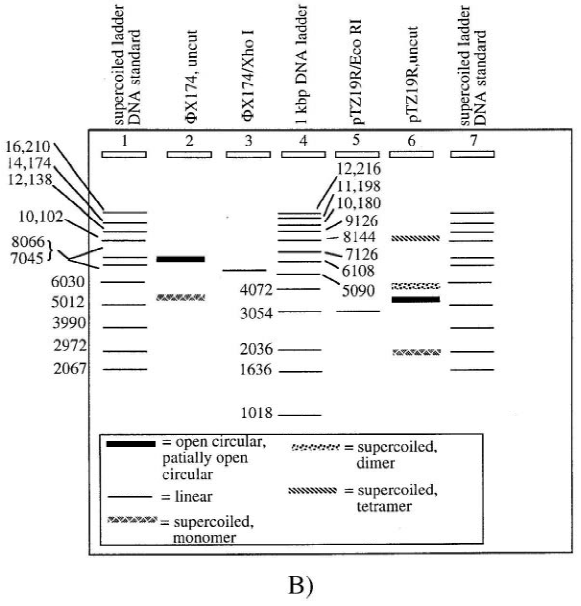

Fig. 1. SGE analysis of DNA ladder standards, ΦX174 plasmid conformers and pTZ19R plasmid conformers in 0.50% (w/w) Trevigel 500 in TAE buffer, pH 8.5. Sample wells are indicated by an arrow. (A) Photograph of gel: lane 1: supercoiled ladder standard, lane 2: ΦX174 plasmid (uncut), lane 3: *Xho*I-digested ΦX174, lane 4: 1 kbp ladder standard, lane 5: *Eco*RI-digested pTZ19R, lane 6: pTZ19R plasmid (uncut), lane 7: supercoiled ladder standard. (B) Schematic of slab gel shown in (A) with DNA fragments labeled in bp.

formation. In support of this observation, the commercial supplier reported that this sample contained approximately 90% supercoiled plasmid. The ΦX174 plasmid was linearized with the restriction endonuclease *Xho*I as described in Section 2.3.2 and electrophoresed (Fig. 1, lane 3). Sizing based on the calibration plot constructed from the 1 kbp ladder standard confirmed its identity (calculated size: 5539 bp, actual size: 5386 bp).

Fig. 2 displays the capillary electrophoretic analysis of the original ΦX174 plasmid sample relative to the supercoiled ladder standard in 0.30% (w/w) HEC-90K in THE buffer, pH 7.3. A predominant single peak was observed. According to calibration sizing using the supercoiled DNA ladder standard, this peak presumably represents the supercoiled conformer. The open circular form was not observed, likely due to sample bias during electrokinetic injection; the larger hydrodynamic radius of this conformer causes it to have a lower electrophoretic mobility [3]. The internal standard dGTP was added to the sample to adjust for run-to-run shifting in electrophoretic mobility; this molecule was chosen based on its negative charge at pH 7.3 and UV absorption at 260 nm. The difference between the migration times of the internal standard and the

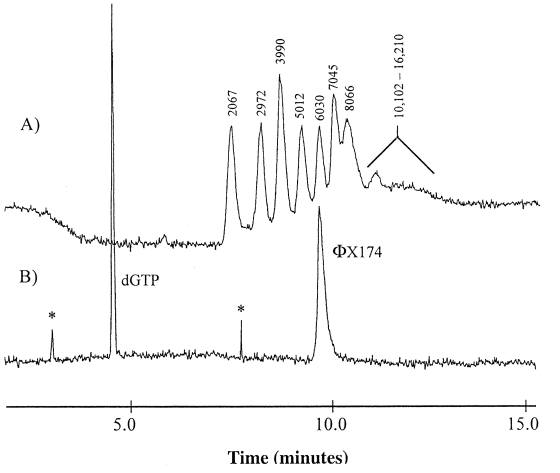

Fig. 2. CE–UV analysis at 260 nm of (A) the supercoiled ladder standard and (B) the ΦX174 plasmid containing dGTP as an internal standard, in 0.30% (w/w) HEC-90K in THE buffer, pH 7.3, at −15 kV (−375 V/cm) at 21°C. DNA fragment sizes of the supercoiled ladder standard are indicated in bp; peaks indicated by an asterisk have not been identified.

analyte were averaged over several electrophoretic runs. This value was added to the average analyte migration time. Then adjusted electrophoretic mobilities were calculated according to Eq. (1),

$$\mu = Ll/Vt \quad (1)$$

where μ is the electrophoretic mobility in $cm^2\ V^{-1}\ s^{-1}$, L is the total capillary length in cm, l is the effective capillary length from the injection end of the capillary to the detection window in cm, V is the applied voltage in V, and t is the migration time in s.

3.2. Analysis of the pTZ19R sample

SGE analysis of the pTZ19R sample revealed a greater complexity overall relative to the ΦX174 sample (Fig. 1, lane 6 versus lane 2). As opposed to the ΦX174 plasmid, which was purchased commercially, the pTZ19R plasmid was isolated in the laboratory. Four bands were observed for the original pTZ19R plasmid sample using SGE, with bands 1 and 2 being the most intense. Band 3 is not readily discernable in Fig. 1A, but was visualized on the UV transilluminator. Bands are numbered as described in Section 3.1. From calibration plots generated using the supercoiled and 1 kbp ladder standards, sample components corresponding to electrophoretic bands were sized. Bands 1, 3 and 4 of the original pTZ19R sample correspond to the supercoiled monomer, dimer and tetramer, respectively. Calculated sizes were 2800 bp (theoretical size: 2870 bp), 5746 bp (theoretical size: 5740 bp), and 11 170 bp (theoretical size: 11 480 bp), respectively. The formation of such catenanes has been discussed previously by Bates and Maxwell [2]. In terms of calibration size, band 2 did not correspond to a supercoiled multimer or to the linear form.

The linear pTZ19R conformer was generated by digestion with *Eco*RI restriction endonuclease at 37°C for 10 min. Comparison of the electrophoretic analysis of this digest (Fig. 1, lane 5) with the original pTZ19R sample (Fig. 1, lane 6) revealed that the latter did not contain a detectable amount of the linear conformer. The pTZ19R plasmid sample was also digested with *Eco*RI at 0°C for 5, 10 and 15 min to induce single-stranded nicks and double-stranded breaks; Na_2EDTA was added as described in Section 2.3.2 in order to halt the enzymatic digestions (data not shown). As the time of treatment with *Eco*RI at 0°C increased, a decrease was observed in the relative amounts of supercoiled multimers. Additionally, an increase in the relative intensity of band 2 was observed concomitantly with the generation of the linear form. Based on the calibration plots and on the observed increase in the intensity of band 2 with increasing digestion time, we suggest that band 2 of the original pTZ19R sample is the fully or a partially open circular form.

Fig. 3 displays the CE separation of pTZ19R sample relative to the supercoiled ladder standard. In general, three peaks were observed for the pTZ19R sample, designated as peaks A, B and C. By comparison with the supercoiled DNA ladder, it was determined that neither peak A nor peak C migrated with the appropriate mobility for the supercoiled conformer or the supercoiled multimers that had been observed in SGE. Peak B exhibited the appropriate migration time for the supercoiled monomer.

A second pTZ19R sample was prepared by replication in the laboratory using competent cells. SGE analysis of this sample revealed a broad smear only; CE analysis revealed a single intense peak (data not

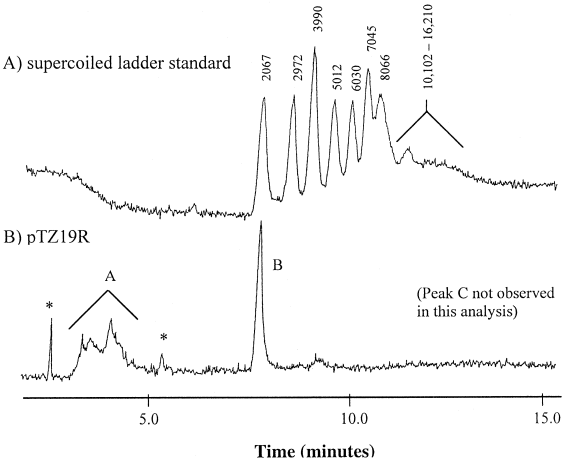

Fig. 3. CE–UV analysis at 260 nm of (A) the supercoiled DNA ladder standard and (B) the uncut pTZ19R plasmid sample. Separation conditions are the same as in Fig. 2. No internal standard was added. DNA fragment sizes of the supercoiled DNA ladder standard are indicated in bp. See text for identification of peaks A and B. Peaks indicated by an asterisk were reproducible but have not been identified.

shown). The latter peak corresponded with peak A of the original pTZ19R sample. We suggest that the second pTZ19R plasmid preparation contained small, linear DNA fragments, generated by multiple double-stranded breaks of the plasmid during the purification process, and/or in the presence of reactive oxygen species. Therefore, we propose that peak A in Fig. 3 is also a distribution of short linear fragments. Such small fragments were not observed in the aforementioned SGE analyses of the pTZ19R plasmid, as they would have presumably migrated off the gel under the experimental conditions used.

Peak C was not observed in every CE analysis. By comparison with the supercoiled ladder in CE, we suggest that peak C does not correspond to the dimer or the tetramer observed in SGE. Peak C, typically observed between 12 and 14 min, is not observed in Fig. 3. However, peak C is observed in Fig. 8. We believe that peak C corresponds to band 2 of Fig. 1, Lane 6, a partially open circular form of the pTZ19R plasmid. The variability of migration time for peak C suggests that the corresponding plasmid conformer is more sensitive to the electrophoretic separation conditions than the conformers corresponding to peaks A and B. We suggest that peak C is not observed in every analysis due to sample bias during electrokinetic injection. It is well established that electrokinetic injection in CE is associated with irreproducibility of sample quantity injected relative to hydrodynamic injection. However, a greater quantity of sample can be injected and peak shapes can be improved using the former. Sample bias does not necessarily result in gradual sample depletion of a particular component over time; in contrast, the quantity of sample injected can increase or decrease from run-to-run. Sample bias is particularly evident in the plasmid samples due to the differences in the relative electrophoretic mobilities of the conformers present. The authors chose to use electrokinetic injection in this case to increase the probability of visualizing as many peaks as possible. Unfortunately, the probability of experiencing irreproducibility of sample quantity injected was increased as well.

A direct comparison of the SGE and CE analyses of the pTZ19R plasmid sample is warranted here. Four bands were observed in the SGE analysis of the pTZ19R sample; whereas, two peaks were observed in the CE analysis. Band 1 of Fig. 1A, lane 6, corresponds to peak B in Fig. 3, the supercoiled monomer. Band 2 of Fig. 1A, lane 6 would have corresponded to peak C in Fig. 3, had that peak been detectable in that run. Peak A in Fig. 3 does not have a correlate in Fig. 1A, lane 6. As indicated previously, such small peaks would have migrated off the gel under these electrophoretic conditions. Band 3 was of too low intensity to be visualized in Fig. 1A, lane 6. The visualization of the correlates to bands 3 and 4 of Fig. 1A, lane 6 in Fig. 3 may have required pulsed field CE. As these data demonstrate, differences exist clearly between the two electrophoretic methodologies under the experimental conditions chosen. CE provides higher separation efficiencies and more reliable quantification; however, SGE provides a better overview of the sample components present. The CE analysis is dependent on the sample injection parameters chosen, as well as the individual electrophoretic mobilities of the sample components. Additionally, in our laboratory, we have noted differences between CE and SGE analyses in relation to the sample matrix (unpublished data); a high ionic strength sample matrix can hinder the injection of sample components and hence hinder the analysis in CE. Therefore, a tradeoff exists for the CE analysis of DNA plasmid molecules. Assuming that the same sample components have been injected in CE and SGE, differences are expected in the two analyses due to the different mechanisms of separation that have been proposed for the different techniques [13,14]. A direct comparison of these two methodologies is not as transparent as one would like. Overall, we believe the advantages of CE outweigh its disadvantages in the analysis of DNA plasmid samples. The selection of the proper analysis technique may be dependent on sample quantities, sample purity, sample matrices, plasmid size and relative quantities of plasmid conformers present in the sample.

3.3. Analysis of the pMD68 plasmid

The pMD68 plasmid sample (27.5 kbp in size) and the *Eco*RI digest of this sample were analyzed using constant field SGE relative to the 1 kbp and supercoiled ladder standards (data not shown). Linear DNA fragments of this size generally require pulsed field electrophoretic techniques for complete analysis

[15]. Additionally, we are not aware of a commercially available plasmid standard encompassing this size range. Nonetheless, a qualitative assessment of the sample components was made. Two bands were observed for the undigested plasmid sample. The first band migrated marginally from the sample wells. The second band co-migrated with the single band observed for the digested samples. The samples contained no detectable levels of DNA fragments less than 12 kbp in size.

The CE separation of the pMD68 sample in 0.30% (w/w) HEC-90K in THE buffer, pH 7.3, is displayed in Fig. 4. Two peaks were observed (peaks D and E). The relatively high mobility of peak D is indicative of a highly compact form. The fine structure of peak D, encompassing peaks 1–5, was highly reproducible. CE analysis of the pMD68/*Eco*RI sample revealed no peaks, as observed for SGE. Analogous to SGE, pulsed-field CE conditions are required for the analysis of DNA molecules in this size range [16,17]. We propose that peak D of Fig. 4 represents a distribution of supercoiled forms of the plasmid, each with different and discrete extents of supercoiling. Recently, Mao et al. demonstrated the CE separation of multiple topoisomers of the pBR322 plasmid generated from treatment with topoisomerase I [9]. In general, plasmids of this size range are organized into several topological domains with defined numbers of supercoils; these domains are secured by a protein or by the attachment to a cellular membrane [1]. The greater mobility of peak D of the presumed supercoiled pMD68 plasmid conformer (27.5 kbp) relative to the supercoiled ladder (2–16 kbp) in CE, may be due to a highly compact structure of the former.

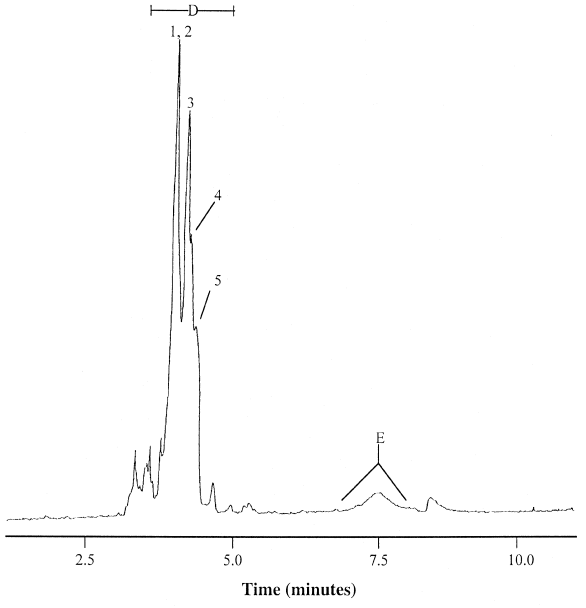

Fig. 4. CE–UV analysis at 260 nm of the pMD68 plasmid (27.5 kbp). Separation conditions are the same as in Fig. 2. No internal standard was added. See text for identification of peaks D and E.

A single-stranded break (a nick) at one of the aforementioned domains of the plasmid molecule is expected to generate unwinding within a discrete region [1,3]. Multiple nicks could increase the hydrodynamic radius of the plasmid by producing several open circular regions; this may substantially slow the electrophoretic migration of this conformer. We believe that peak E in Fig. 4 represents the product of such nicking. The broadness of the peak suggests a distribution of partially open circular forms. This CE peak may correspond to the SGE band that migrated marginally from the sample wells in the undigested samples; its relatively low mobility further suggests an open circular conformation [1,3].

3.4. Analysis of irradiated ΦX174 samples

The ΦX174 plasmid was exposed to 50, 100 and 200 Gy doses of γ-radiation. The irradiation doses employed in the present investigation were chosen based on previously reported data for irradiation of linear DNA fragments [5]. The irradiated samples were analyzed initially using the CE–UV system. The dGTP internal standard was added after irradiation. Separations were performed in 0.3% (w/w) HEC-90K in THE buffer, pH 7.3. A single, broad peak was observed for all analyses (data not shown). The peak width was measured at one-half height, and the peak width increased with increasing radiation dose. Peak width at one-half height has been used previously in CE–LIF for monitoring damage in linear DNA fragments [5,18]. A plot of peak distribution (width in s) versus radiation dose (in Gy) is shown in Fig. 5. In general, an increase in peak width at half height was observed with increasing radiation dose.

SGE analysis of the irradiated plasmid samples revealed two predominant bands (Fig. 6, lanes 3–5).

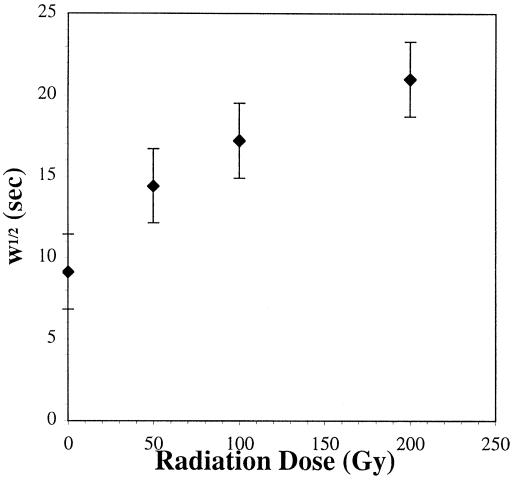

Fig. 5. Peak width at one-half peak height ($w_{1/2}$) (in s) as a function of radiation dosage (in Gy) for the ΦX174 plasmid sample. All experiments were performed using the CE–UV system. Error bars indicate standard deviations.

The bands are numbered as described in Section 3.1. No significant quantities of the supercoiled form remained after exposure to γ-radiation of 50 Gy or greater. This is evidenced by the fact that a distinct electrophoretic band corresponding to band 1 of the unirradiated ΦX174 plasmid sample (see Fig. 6, lanes 2 and 6) was not observed in any of the irradiated samples. Band 1 of the irradiated samples (Fig. 6, lanes 3–5) corresponds with the linear form according to a calibration curve constructed from the 1 kbp ladder standard. Band 2 of the irradiated samples corresponds to the less intense band 2 of the unirradiated samples, and does not correspond to the linear form or to a supercoiled multimer. Presumably, band 2 of both the irradiated and unirradiated samples represents the open circular form. A distinct trail from the leading edge of band 1 in Fig. 6, lanes 4 and 5, which we believe to be a distribution of small linear fragments, increased with radiation dose. Based on these results, we suggest that the tailing

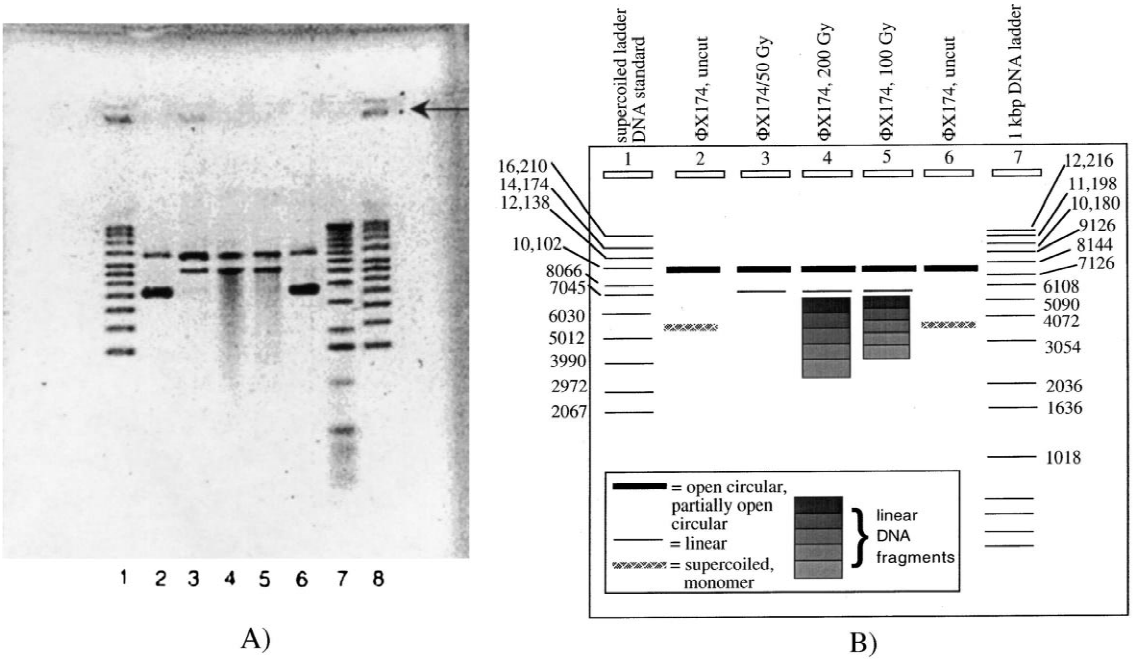

Fig. 6. SGE analysis of the ΦX174 plasmid (uncut), irradiated ΦX174 plasmid samples, and DNA ladder standards in 0.50% (w/w) Trevigel 500 in TAE buffer, pH 8.5. Sample wells are indicated by an arrow. (A) Photograph of gel: lane 1: supercoiled DNA ladder standard, lane 2: ΦX174 plasmid (uncut), lane 3: ΦX174 plasmid exposed to 50 Gy γ-radiation, lane 4: ΦX174 plasmid exposed to 200 Gy γ-radiation, lane 5: ΦX174 exposed to 100 Gy γ-radiation, lane 6: ΦX174 plasmid (uncut), lane 7: 1 kbp DNA ladder standard, and lane 8: supercoiled DNA ladder standard. (B) Schematic of slab gel shown (A), with the exception of lane 8 for simplicity. DNA fragments labeled in bp.

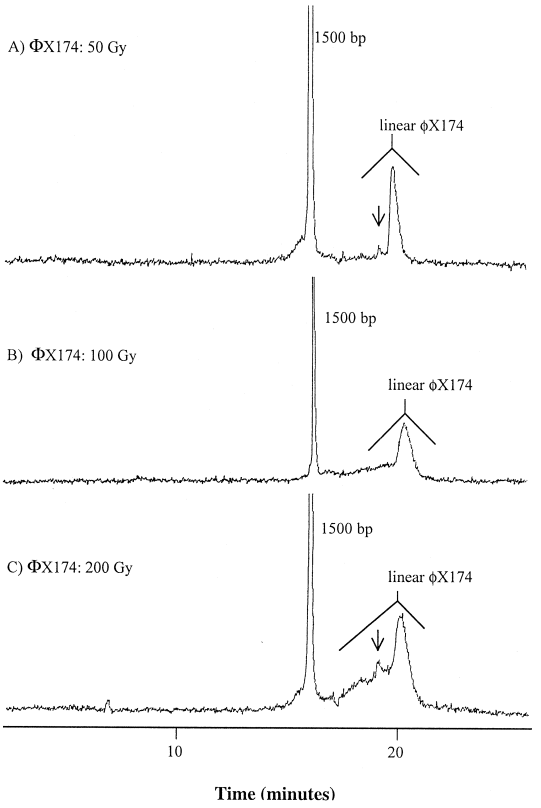

Fig. 7. CE–LIF analysis of γ-irradiated ΦX174 plasmid samples in 0.30% (w/w) HEC-90K in THE buffer, pH 7.3, containing 100 ng/ml YO-PRO-1, at −15 kV (−250 V/cm) at 30.0°C: (A) 50 Gy, (B) 100 Gy, and (C) 200 Gy. The 1500 bp internal standard was added after irradiation. The migration time of the peak indicated by an arrow was reproducible.

peaks observed in CE represent a distribution of linear fragments that are shorter in length than the original linear conformer.

Due to room temperature fluctuations, greater run-to-run shifting in migration times (4.3% RSD) was observed during the CE–UV analysis of these irradiated samples relative to other analyses presented herein. Previously, we have achieved greater run-to-run reproducibility with the CE–LIF system due to the superior temperature control of the ATI Unicam CE unit compared to that of the CE–UV system. Therefore, in order to size accurately the dsDNA fragmentation products, the irradiated samples were analyzed using the CE–LIF system in the presence of 100 ng/ml of the intercalating dye YO-PRO-1 (Fig. 7). Instead of dGTP as an internal standard, a 1500 bp linear DNA fragment was added after irradiation. The former neither exhibits native fluorescence excitable by the Argon ion laser, nor participates in intercalating interactions in a significant manner. The addition of an intercalating dye to the CE separation medium is expected to induce conformational changes in circular DNA molecules, especially supercoiled conformers [3]. Therefore, the analysis of the unirradiated ΦX174 plasmid sample was not conducted. Single-stranded DNA fragmentation products were produced possibly during irradiation, but YO-PRO-1 has a relatively low affinity for single-stranded DNA [19]. As a result, it was anticipated that such peaks would not be observed in the CE–LIF analysis. DNA fragmentation products were sized according to the calibration curve constructed from the 1 kbp ladder standard (Table 1). Run-to-run shifting in migration times was adjusted using the migration times for the 1500 bp internal standard in a manner analogous to that described previously for the dGTP internal standard (Section 3.1). The discrepancy in sizing the predominant fragmentation product of the irradiated ΦX174 plasmid sample in SGE versus CE cannot be explained at this time. The migration times for the peaks indicated by arrows in Fig. 7A and C were highly reproducible; the calculated DNA fragment sizes corresponding to these peaks are also listed in Table

Table 1
Migration times of CE peaks and calibrated sizes of corresponding DNA fragments of the irradiated ΦX174 plasmid samples[a]

Sample	Average migration time, major peak (min)	Fragment size (bp)	Average migration time, minor peak (min)	Fragment size (bp)
ΦX174/50 Gy	20.31	3650	19.96	3017
ΦX174/100 Gy	20.60	4191	***	***
ΦX174/200 Gy	20.62	4280	20.08	3071

[a] CE separation conditions are the same as indicated in Fig. 2.
*** Indicates that data could not be determined.

1. The peaks correspond to 3017 bp in the ΦX174/50 Gy sample and 3071 bp in the ΦX174/200 Gy sample. This particular fragmentation product presumably represents an energetically favored cleavage site; however, the physical significance of this site is undetermined at this time. Similarly distinct electrophoretic peaks were observed in the analysis of γ-irradiated linear DNA fragments [5]. We propose that for the ΦX174/100 Gy sample, this peak may have been present in solution, but was obscured by the distribution of DNA fragments as well as baseline noise (Fig. 7B).

3.5. Analysis of irradiated pTZ19R samples

The pTZ19R plasmid was exposed to 50, 100 and 200 Gy of γ-radiation as well. Irradiated samples of this 2870 bp plasmid displayed a trend in peak broadening similar to that observed for the ΦX174 plasmid, especially peak B (Fig. 8). The baseline shift shown in Fig. 8D was not reproducible. Peak B, representing the supercoiled monomer, showed a substantial increase in peak width upon exposure to 50 Gy of γ-radiation, and was increasingly undetectable at higher doses. There was an increase in area of peak A with increasing radiation dosage; this observation agrees with the previous assertion that this peak represents a distribution of small, linear DNA fragments (Section 3.2). Peak C, representing the open circular form of the original ΦX174 plasmid sample, was the least reproducible, with variable peak areas and migration times. SGE analysis of the irradiated pTZ19R plasmid samples was limited by sample concentration; unresolved bands of relatively

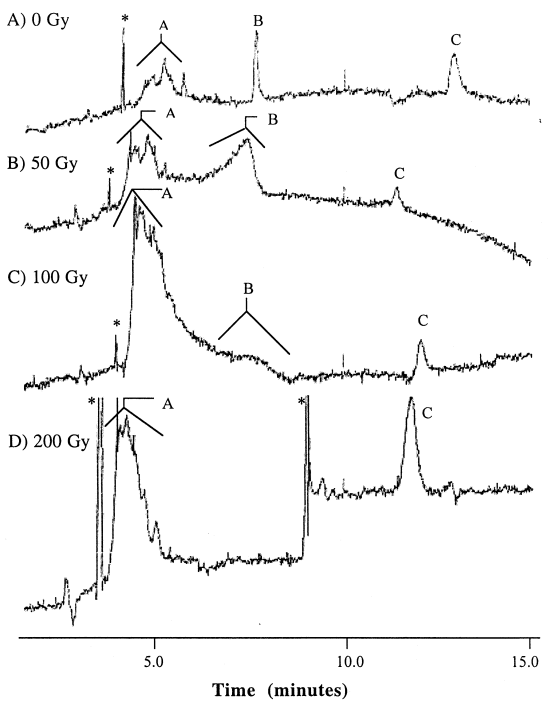

Fig. 8. CE–UV analysis at 260 nm of unirradiated and γ-irradiated pTZ19R samples: (A) 0 Gy, (B) 50 Gy, (C) 100 Gy, and (D) 200 Gy. Separation conditions are the same as in Fig. 2. No internal standard was added. Peaks indicated by an asterisk were reproducible but have not been identified.

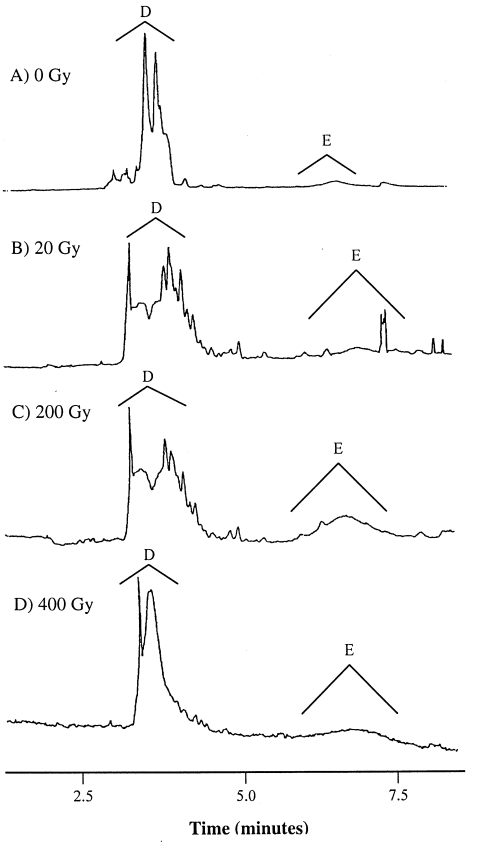

Fig. 9. CE–UV analysis at 260 nm of unirradiated and γ-irradiated pMD68 samples: (A) 0 Gy, (B) 20 Gy, (C) 200 Gy, and (D) 400 Gy. Separation conditions are the same as in Fig. 2. No internal standard was added. See text for identification of peaks D and E.

low intensity were observed for all irradiated samples (data not shown).

3.6. Analysis of irradiated pMD68 samples

The pMD68 plasmid sample was exposed to higher radiation dosages (up to 400 Gy) than the other two plasmid samples due to the greater size of the former. Fig. 9 displays the CE separation of the irradiated pMD68 plasmid samples. The fine structure of peak D in Fig. 9 was highly reproducible for each individual irradiated sample. Relative to the unirradiated plasmid sample, the width of peak D increased significantly upon exposure to 200 Gy radiation, but decreased significantly upon exposure to 400 Gy radiation. We propose that the increase in peak width at the two lower doses corresponds to the conversion of discrete supercoiled conformers to a wider distribution of supercoiled conformers with varying levels of supercoiling. The decrease in width of peak D at the highest radiation dose may correspond to the generation of the fully linear form and/or the fully open circular form. It is unlikely that either of these conformers would be observed without pulsed field CE [16,17]. We recognize that double-stranded breaks may also generate small, linear fragments.

4. Conclusions

We have demonstrated the applicability of dynamic size-sieving CE for the detection of γ-irradiation-induced fragmentation products of plasmids ranging in size from 2.8 to 27.5 kbp. SGE was used in conjunction with CE as an aid in the sizing and identification of DNA sample components. The data obtained using SGE were complementary in several instances to the data obtained using CE. However, CE provides greater separation efficiency and higher detection sensitivity than SGE. Conformers that were represented as single bands or smears in SGE were represented as partially resolved peaks in CE, with highly reproducible electrophoretic peak patterns. In some instances, peak broadening as a function of radiation dosage was used to assess the presence of various DNA fragmentation processes. The analysis of unirradiated and irradiated plasmid samples using CE–UV at 260 nm in the absence of DNA intercalating dyes reduces the likelihood of undesirable conformational changes within the plasmid molecules. Combined with the capacity of CE for single-cell analysis, this technique may afford quantitative and highly localized analysis of radiation effects. The investigation of radiation effects in CE could be extended to examine fragmentation products produced in the presence of radiosensitizers and radioprotectors, which may further the development of more effective radiotherapies. Additionally, future investigations of the utilization of repair enzymes specific for each irradiated plasmid would be insightful.

Acknowledgements

The authors wish to thank the Jeffress Memorial Trust Foundation (Grant No. J-362) for financial support of this work, as well as the Department of Chemistry at the College of William and Mary for two summer research stipends for S.A.N.

References

[1] R.S. Sinden, in: DNA Structure and Function, Academic Press, San Diego, CA, 1994, Chapter 3.
[2] A.D. Bates, A. Maxwell, in: DNA Topology, Oxford University Press, New York, 1993, Chapters 2, 4 and 6.
[3] P.H. Johnson, L.I. Grossman, Biochemistry 16 (1977) 4217–4224.
[4] B.M. Sutherland, P.V. Bennett, K. Conlon, G.A. Epling, J.C. Sutherland, Anal. Biochem. 201 (1992) 80–86.
[5] B.A. Siles, Z.E. Nackerdien, G.B. Collier, J. Chromatogr. A 771 (1997) 319–329.
[6] Z. Nackerdien, S. Morris, S. Choquette, B. Ramos, D. Atha, J. Chromatogr. B 683 (1996) 91–96.
[7] D.W. Fairbairn, P.L. Olive, K.L. O'Neill, Mut. Res. 339 (1995) 37–59.
[8] M. Klaude, S. Eriksson, J. Nygren, G. Ahnstrom, Mut. Res. 363 (1996) 89–96.
[9] D.T. Mao, J.D. Levin, L. Yu, R.M.A. Lautamo, J. Chromatogr. B 714 (1998) 21–27.
[10] E.N. Fung, E.S. Yeung, Anal. Chem. 67 (1995) 1913–1919.
[11] B.A. Siles, D.A. Anderson, N.S. Buchanan, M.F. Warder, Electrophoresis 18 (1997) 1980–1989.
[12] G.A. Ross, J. Chromatogr. A 718 (1995) 444–447.

[13] A.E. Barron, H.W. Blanch, D.S. Soane, J. Chromatogr. A 652 (1993) 3–16.
[14] N.C. Stellwagen, Biochemistry 221 (1983) 6186–6193.
[15] M. Wang, E. Lai, Electrophoresis 16 (1995) 1–7.
[16] Y. Kim, M. Morris, Electrophoresis 17 (1996) 152–160.
[17] J. Sudor, M.V. Novotny, Anal. Chem. 66 (1994) 2446–2450.
[18] M.D. Evans, J.T. Wolfe, D. Perrett, J. Lunec, J.E. Herbert, J. Chromatogr. A 700 (1995) 151–160.
[19] R.P. Haugland, in: Handbook of Fluorescent Probes and Research Chemicals, Molecular Probes, Eugene, OR, 1996, pp. 143–174.